Quantum chemical study of substituent effect on CN bond in aryl isocyanide molecules adsorbed on the Pt surface

Ben Wang,[†] Min Gao,[§] Kohei Uosaki,[$] and Tetsuya Taketsugu[‖,‡,*]

[†]Graduate School of Chemical Sciences and Engineering, Hokkaido University, Sapporo 060-0810, Japan

[§]Institute for Catalysis, Hokkaido University, Sapporo 001-0021, Japan

[$]International Center for Materials Nanoarchitectonics (MANA), National Institute for Materials Science (NIMS), Tsukuba 305-0044, Japan

[‖]Department of Chemistry, Faculty of Science, Hokkaido University, Sapporo 060-0810, Japan

[‡]Institute for Chemical Reaction Design and Discovery (WPI-ICReDD), Hokkaido University, Sapporo 001-0021, Japan

ABSTRACT:

A periodic implemented scheme of natural bond orbital (NBO) theory and normal mode analysis have been employed to investigate a chemical bond strength tendency for aryl isocyanide molecules with different *para*-substituted groups adsorbed on the Pt(111) surface. The NC bond order shows a clear correspondence with the NC stretching frequency; both of them exhibit a "volcano-like" profile as a function of the Hammett constant of the *para*-substituted groups for isolated molecules. When the molecule adsorbs on the Pt(111) surface, the NC stretching frequency variations is determined by the resultant effect of σ donation and π back-donation between the molecule and surface. The present comprehensive and systematic computations clarify the electron donating and withdrawing effect of the substituted groups on the interaction between aryl isocyanide molecule and the transition metal substrate.

KEYWORDS: Natural bond orbital, adsorbate/surface interaction, donation and back-donation

INTRODUCTION

In the last decade, there has been a large growth of research efforts in the field of molecular electronic devices.[1–4] Self-assembled monolayer (SAM) is a major area of interest concerning fabricating molecular electronic devices.[5–11] A crucial aspect for the application of these SAMs in electronic devices is their interface formation with the metal surface at the contacting electrodes, providing a unique tool for probing the charge transport processes on the nanoscale. Besides the most extensively investigated system–sulfur derivatives, such as thiol SAMs on gold electrodes,[12–20] aryl and alkyl isocyanides[20–30] have also received considerable attention. The electronic properties of the metal−organic interfaces can determine the essential performance parameters. Thus, evaluating the conduction behavior of the molecule−metal junction accurately is a continuing concern within the improvement of molecular electronic devices.

In addition to the conductance data, the conduction behavior at the metal−molecule−metal junction is strongly influenced by the nature of molecular bonding and conformation at the electrode surface. The resonant frequency based vibrational spectroscopy is one of the most widely used techniques for identifying this bonding information, and a frequency shift for the adsorbed molecule on the surface can be used to investigate a chemical bonding nature on the surface. Uosaki *et al*. reported the substrate dependence of aryl isocyanide molecules adsorbed on the metal surface by the sum frequency generation (SFG) spectroscopy.[22] The effect of a *para*-substituted group of aryl isocyanides and metal substrates on the SFG spectrum were also investigated. For examining a bonding nature between NC terminal group and substrate atoms, tilt angles of 4-methylphenyl isocyanide (MPI) were estimated from the intensity ratio between SFG peaks of C−H symmetric and asymmetric stretching vibrational modes of CH_3 group. However, a nature of bonding between aryl isocyanide molecule and metal substrates is still not intuitional.

For understanding a bonding nature more intuitively, various methods have been used to quantitatively examine the electron transfer between the molecule and surface. Hu *et al*. employed an overlap population of molecular orbitals (MOs) to elucidate the magnitude of interaction between 4-chlorophenyl isocyanide molecule and Au(111) or Pt(111) surface and the relationship between the vibrational spectra and the electronic structure quantitatively.[30] Besides, two topological approaches, Bader's quantum theory of atoms-in-molecule (QTAIM)[31–34] and electron localization function (ELF),[35,36] are broadly accepted as the modern theoretical tools for studying the nature of interactions. QTAIM connects the topology of a system's electron density to the conception of atoms and chemical bonding, while ELF provides information on the bonding type, including covalent, ionic, or metallic bonds. Additionally, due to the close association with the elementary Lewis structure diagrams, natural bond orbital (NBO) analysis is widely used in deciphering the chemical bonding to interpret the electronic structures of molecules.[37] In the NBO method, bonding orbitals, antibonding orbitals, and lone pair orbitals are constructed as the linear combinations of orthogonal hybrid orbitals centered on atoms within the molecule. The NBO approach has been used for isolated molecular systems, but recently it is extended to a periodic system by Dinnington and Schmidt.[38] The periodic implemented NBO theory has been applied to various problems such as the CO adsorption site preference,[39] geometric changes occurring upon the removal of a single O atom from the MgO surface,[40] and reaction mechanism of catalytic NO oxidation by Cr_2O_3.[41] In this study, we employ the periodic implemented NBO analysis to examine substituent effect on the bonding nature for aryl isocyanide molecules adsorbed on the metal surface. Vibrational frequencies were also calculated to get insight into the NC chemical bond strength.

COMPUTATIONAL DETAILS

The density functional theory (DFT) calculations were performed for the aryl isocyanide molecules X−C_6H_4−NC (X = $N(CH_3)_2$, NH_2, OCH_3, CH_3, H, Cl, CF_3, CN, NO_2) as isolated ones and on the Pt(111) surface in the framework of the generalized Kohn-Sham scheme using the projector augmented-wave (PAW)[42,43] method as implemented in the Vienna Ab-Initio Simulation Package (VASP) code.[44–47] The calculations employ the Perdew-Burke-Ernzerhof (PBE)[48,49] exchange-correlation functionals and account for dispersion interactions using DFT-D3.[50–52] The parameters were directly taken from the implementation of dispersion in DFT calculation. For Pt atom, the valence s and d electrons and semicore p electrons were treated as valence electrons. The convergence criteria for the total energy was set to 10^{-5} eV. Geometry optimization was performed until the maximum final force becomes less than 0.025 eV/Å using a conjugate-gradient algorithm. The Γ-centered 9 × 9 × 1 meshes of the **k** grid, generated according to the Monkhorst-Pack scheme,[53] was applied to the Brillouin zone (BZ) integrations, with a plane wave cutoff energy E_{cutoff} = 600 eV. Only Γ point (1 × 1 × 1) was employed for isolated molecule.

The lattice constant of the bulk metal was obtained by fitting to the second-order Birch-Murnaghan equation of state;[54] computed lattice constant of 3.9197 Å is in good agreement with the experimentally determined 3.9242 Å.[55] The Pt(111) surface was modeled with a 2 × 2 super cell and four-layered slabs. A vacuum thickness with at least 14 Å was used to sufficiently eliminate the periodic image interactions. For the pure Pt(111) surface, only the top two layers were allowed to relax. Once the convergence was reached, X−C_6H_4−NC molecule was placed at the top site. The C atom was positioned above one Pt atom, and the N−C bond was oriented perpendicular to the surface, which is consistent with the experimentally observed atop adsorption site.[22] Finally, the coordinates of the atoms in the bottom two layers were fixed while the adsorbed

molecule and the upper two layers of the Pt surface were fully relaxed. Spin polarization was turned on in all calculations.

The vibrational frequencies were calculated using a finite difference approach with a displacement of 0.015 Å where all atoms of the molecule and only one Pt atom directly bound to the molecule were included to reduce a computational cost.

The periodic NBO analysis requires the electronic wave function represented in atom-centered basis functions. So we projected the plane wave function into the Gaussian-type basis functions taken from the EMSL basis set library.[56,57] In this analysis, triple-ζ 6-311G* basis set was employed for C, H, N, O, F,[58] and Cl atoms,[59] while jorge-DZP basis set was utilized for Pt.[60] Visualization of the structures and NBO results were achieved with the help of Visualization for Electronic and Structural Analysis (VESTA) software.[61]

To further quantify a covalent and metallic nature of the chemical bonding, we also projected a plane wave solution to local orbital basis functions to extract crystal orbital Hamiltonian population (COHP) which was achieved by using the program of Local-Orbital Basis Suite Towards Electronic-Structure Reconstruction (LOBSTER)[62–64] based on the output files of single VASP static run. The ELF analysis was also carried out to examine the bonding type for the molecule and surface. The results are summarized in the Supplementary Information.

RESULTS AND DISCUSSION

Bond order and vibrational frequency in isolated X−C_6H_4−NC molecule.

Table 1 lists nine substituents (X) studied in this work, with their corresponding *para*-substituted Hammett constants (σ_p),[65,66] which have been used to evaluate the electron donating/withdrawing ability of a *para*-substituted group on the directly bonded benzene ring through resonance. Electron-donating groups (EDG) possess negative σ_p values, whereas electron-withdrawing groups (EWG) possess positive σ_p values. X = H is treated as a reference substituent as $\sigma_p = 0$.

Table 1. Substituents set *para* to the aromatic ring in the aryl isocyanide molecules along with the corresponding Hammett constant (σ_p) for each substituent.

−X	σ_p	−X	σ_p
$-N(CH_3)_2$	−0.83	−Cl	0.23
$-NH_2$	−0.66	$-CF_3$	0.54
$-OCH_3$	−0.27	−CN	0.66
$-CH_3$	−0.66	$-NO_2$	0.78

Figure 1 shows several NBOs related to the NC bonding of an isolated H−C_6H_4−NC molecule. The σ and doubly degenerate π bonding orbitals constitute the triple bond of the NC bond. When considering the planarity of the benzene ring, π orbitals of NC can be divided into the vertical (out-of-plane) component (π_{vert}), and the parallel (in-plane) component (π_{para}). Figure 1 also shows the C lone pair orbital with doubly-occupation, which is a hybridized orbital consisting of C 2s (~70 %) and C $2p_z$ (~30 %), and three antibonding orbitals. It is noted that the C lone pair orbital has a slight antibonding character between C and N atoms.

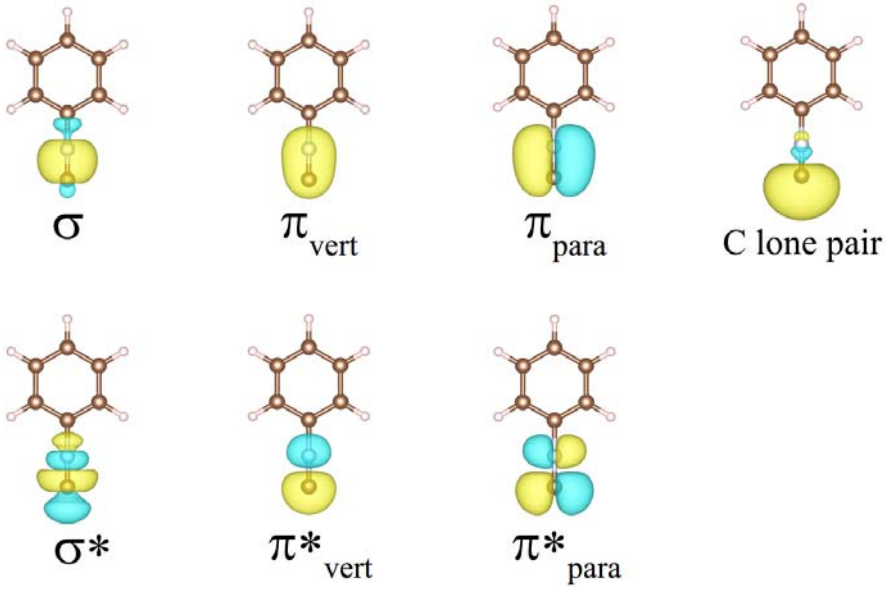

Figure 1. The NBOs related to the NC bonding nature in isolated H−C_6H_4−NC molecule: σ bonding orbital, vertical component of π bonding orbital (π_{vert}), parallel component of the π bonding orbital (π_{para}), C lone pair orbital, and the corresponding three antibonding orbitals. Isosurface corresponds to 0.04 e/Bohr^3.

To evaluate the NC bond strength, we employ a bond order defined as

$$(n_{BO} - n_{ABO}) / 2 \quad (1)$$

where n_{BO} and n_{ABO} denote the numbers of electrons in the bonding orbitals and antibonding orbitals, respectively. The bond order is not observable, but rather a tool or model for better understanding of chemical bonding strength based on the electronic wavefunction. The bond strength can also be examined by the NC stretching frequency: a stronger bond corresponds to a higher frequency and vice versa. **Figure 2** shows the calculated results of (a) NC stretching frequency, (b) NC bond order, (c) NC bonding orbital population, and (d) NC antibonding orbital population for isolated X−C_6H_4−NC molecules as a function of the Hammett constants. The bond

orders and orbital populations were determined from the NBO analysis. As shown here, both the NC stretching frequency and NC bond order have the same "volcano-like" profile: they both tend to increase from the most EDG to H and tend to decrease from H to the most EWG.

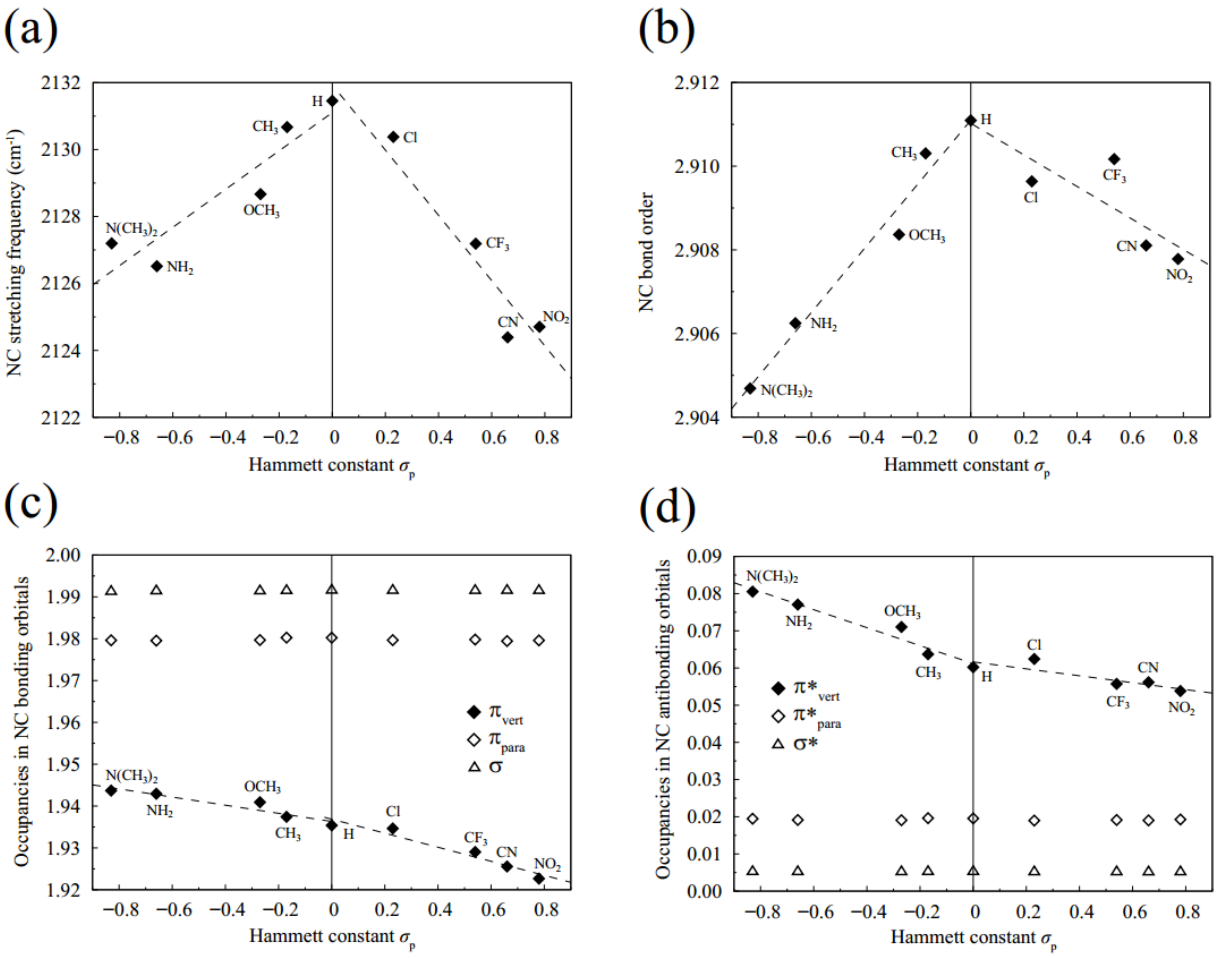

Figure 2. The calculated results for isolated X−C_6H_4−NC molecules: (a) NC stretching frequency, (b) NC bond order, (c) NBO occupancies in NC bonding orbitals (σ and π), and (d) NBO occupancies in NC antibonding orbitals (σ* and π*) for isolated X−C_6H_4−NC molecules, as a function of the Hammett constants.

It is realized that electron transfer between the *para*-substituted group and NC part in isolated aryl isocyanide molecules accounts for changes in the NC bond order. The EDG works to increase electron denstity in benzene ring by resonance, resulting in more electron transfer into the antibonding orbital of NC. On the other hand, EWG works to withdraw electron from the benzene ring, resulting in partial removal of electron from the NC bonding orbitals. For more detailed analysis, we evaluated NBO occupancies in σ, π_{vert}, and π_{para} orbitals, separately. **Figures 2c and 2d** depict variations of occupancies of the bonding and antibonding orbitals, respectively. As expected, the occupancies in the σ and π_{para} bonding orbitals are found to be roughly constant with respect to the electron withdrawing and donating ability of substituents. In contrast, the occupancies in the π_{vert} bonding orbital are significantly affected so that occupancies in π_{vert} decrease from 1.94 (X = $N(CH_3)_2$) to 1.92 (X = NO_2). In all cases, a substantial decrease is observed in π_{vert} bonding orbital population along with the increase of the withdrawing ability and the decrease of the donating ability. Thus, electron transfer to *para*-substituted group is mainly due to electron loss in π_{vert} bonding orbital on NC. On the other hand, electron transfer from the *para*-substituted group to NC group can be quantified from population changes in three corresponding antibonding orbitals, σ*, π^*_{para} and π^*_{vert}, as shown in Fig. 2d. Again, it is found that occupancies in σ* and π^*_{para} antibonding orbitals keep fairly invariant through a whole range of the Hammett constants, and electron transfer into these orbitals is very limited. In contrast, the decreasing trend of occupancy is observed in π^*_{vert} antibonding orbital; substituent with the greater electron donating ability pushes more electrons into π^*_{vert} orbitals, indicating that π^*_{vert} is much more sensitive to the electron withdrawing and donating ability.

Summarizing the above results, variation in the bond order in Fig. 2b is primarily due to change in π_{vert} component, and the overall bond orders follow the pattern of the π_{vert} and π_{vert}*

occupancies. More subtly, the continuous decreases in the occupancy of π_{vert} and π^*_{vert} orbitals are different toward each other. As for the occupancy of π_{vert} orbital, a plotted line in EDG part exhibits a gentle slope compared to the other half in the EWG part. Contrarily, the decreasing trend in the occupancy of π^*_{vert} orbital is completely opposite. Clearly, this difference invokes the overall "volcano-like" trend of the bond order.

The "volcano-like" trend of the bond order could be explained qualitatively by considering that EDGs donate electron to the antibonding orbitals through the benzene ring, while EWGs withdraw electron from the bonding orbitals. Both of these two ways lead to a decrease of the bond order, and thus, a molecule with no substitution case ($H-C_6H_4-NC$) has the highest bond order. Of course, the local populations are reasonably affected by the substituent (see **Fig. S1** in SI). As the electron-withdrawing ability of the substituent increases, C atom is more positively charged, while N atom becomes more negative. This also confirms the occurrence of electron transfer from C to N, benzene ring, and X group, which is caused by the electron-withdrawing ability of the *para*-substituted group.

X−C_6H_4−NC adsorbed on the Pt(111) surface.

Hence, we turn to the aryl isocyanide molecules adsorbed on the Pt(111) surface. It is known that the prediction of the adsorption site remains a challenging subject for standard DFT computation in the case of CO adsorption on the transition metal surface.[67–71] Actually, our DFT calculations with PBE functional predicted the adsorption site of X−C_6H_4−NC molecule on the Pt(111) surface as the hollow site, although the experiment indicated that the molecule adsorbs at the atop site.[22] In the present calculation, N−C bond was oriented perpendicular to the Pt(111) surface, according to the experimental report. **Figure 3** shows the top and side views of the optimized geometry of H−C_6H_4−NC molecule adsorbed on the Pt(111) surface. **Figure 4** shows the variations of NC stretching frequency and NC bond order for X−C_6H_4−NC molecule (X = $N(CH_3)_2$, NH_2, OCH_3, CH_3, H, Cl, CF_3, CN, NO_2) as isolated molecules (black) and those on the Pt(111) surface (red), as a function of the Hammett constant. As shown in Fig. 4a, the introduction of surface effect increases the NC stretching frequency by ~70 cm^{-1} (blue shift) compared with the corresponding isolated molecules, which is consistent with the experimental SFG results.[22] This result indicates that electron transfer between the molecule and surface can affect the NC stretching frequency largely. In particular, different from the previous "volcano-like" trend for isolated molecule, the NC stretching frequency after adsorption shows a decreasing trend, and the slope in the EWG region with positive σ_p is steeper than that in the EDG region with negative σ_p.

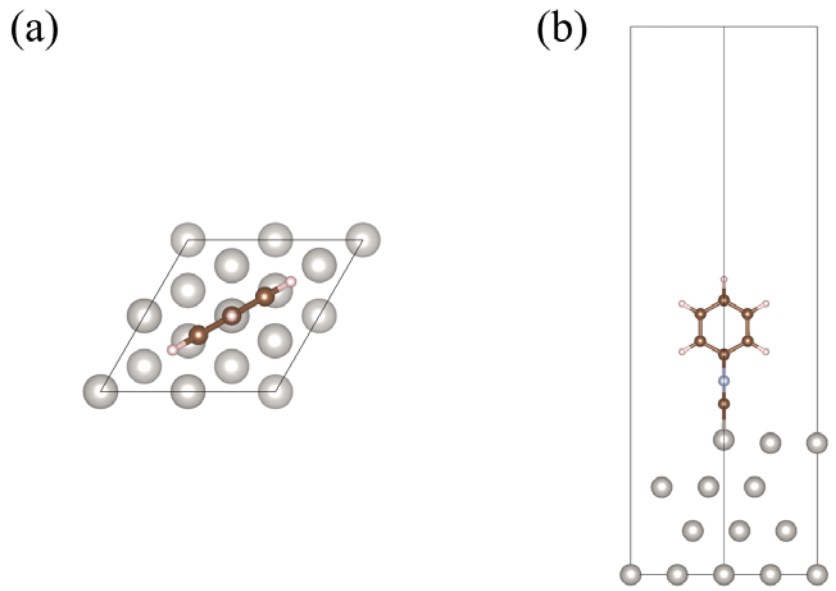

Figure 3. Schematic configuration of (a) top and (b) side views of X−C_6H_4−NC molecule adsorbed on the Pt(111) surface, with a coverage of 1/4.

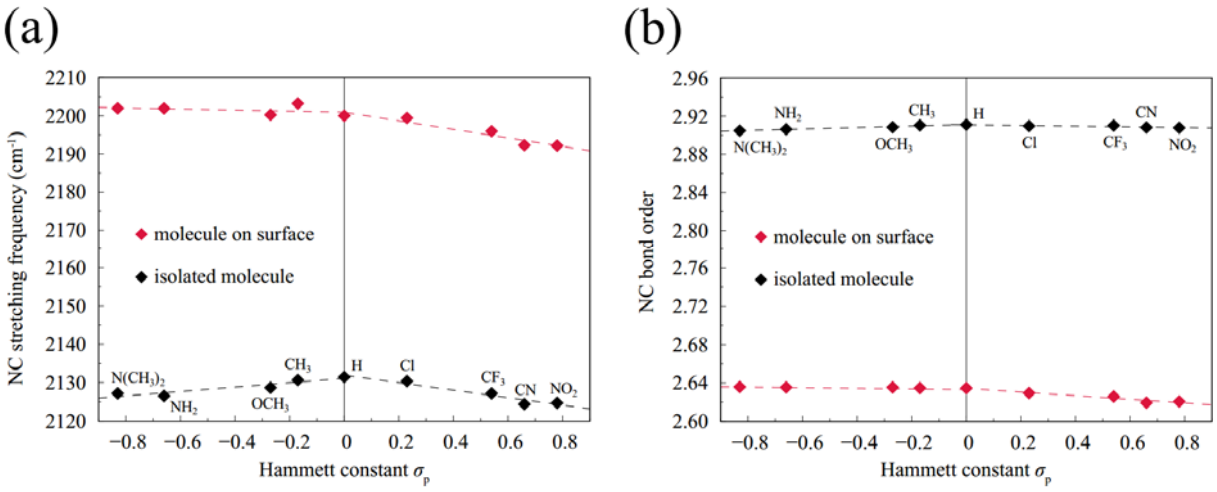

Figure 4. Variations of (a) NC stretching frequency and (b) NC bond order, plotted for X−C_6H_4−NC molecules as an isolated molecule (black), and those adsorbed on the Pt(111) surface (red) as a function of Hammett constant. The dashed lines represent the linear fit for the respective positive and negative regions of the Hammett constants.

Figure 4b depicts the NC bond order for isolated and adsorbed X−C_6H_4−NC molecules. It is interesting to note that, although the NC stretching frequency shows a blue-shift by ~70 cm^{-1} after adsorption, the NC bond order decreases by 0.28. Thus, the larger bond order does not always indicate the higher frequency of the corresponding stretching vibrational mode. The bond orders for the isolated molecules show a "volcano-like" profile, while those for the adsorbed molecules show a decreasing tendency from 2.64 to 2.62, which can be intuitively explained by electron transfer from the Pt surface to the NC antibonding orbitals. Similar to the NC stretching frequency trend, we found the slope in the EWG region is also steeper than that in the EDW region. According to the given definition of NBO bond order, this trend is ascribed to a larger increase in the antibonding orbital occupancy over a smaller decrease in the bonding orbital occupancy.

Table 2. NC bond length of X−C_6H_4−NC molecules adsorbed on Pt(111) surface and the adsorption energies.

	Hammett constant	NC bond length (Å)	Adsorption energy, E_{ads} (eV)
$N(CH_3)_2$	−0.83	1.1827	−2.4315
NH_2	−0.66	1.1829	−2.4281
OCH_3	−0.27	1.1833	−2.5042
CH_3	−0.17	1.1831	−2.4590
H	0	1.1837	−2.4277
Cl	0.23	1.1840	−2.4621
CF_3	0.54	1.1849	−2.4693
CN	0.66	1.1855	−2.3526
NO_2	0.78	1.1851	−2.3758

Table 2 lists the NC bond length of X−C_6H_4−NC molecules adsorbed on Pt(111) surface and the respective adsorption energies defined as

$$E_{ads} = E[\text{molecule-surface}] - (E[\text{molecule}] + E[\text{surface}]) \quad (2)$$

in which $E[A]$ denotes the calculated electronic energy of A. With the increase of the electron withdrawing ability, NC bond length increases. In contrast, adsorption energies show a fluctuation from −2.35 to −2.50 eV.

To get insight into the origin of the similar tendency in NC stretching frequency and bond order variations, we would focus on the factors that directly affect the bonding mechanism. Therefore, we examine the electron transfer process during the formation of a chemical bond between X−C_6H_4−NC molecule and Pt surface. Such electron transfer introduces a spectroscopic change of aryl isocyanide molecules on metal surfaces.[22,23,30,72] The Blyholder model consisting of σ donation and π back-donation have been commonly used to describe an interaction between CO molecule and Pt(111) surface.[39,73−75] The validity of Blyholder-type arguments has also been confirmed for other models, for instance, HNC on the Au(111) surface,[76] and Cl−C_6H_4−NC on Au(111) and Pt(111) surfaces,[30] Cl−C_6H_4−NC on Pt(110), Pt(211), Pt(100), and Pt(111).[23] Here, we employ the σ donation/π back-donation model in which the NC bond strength of X−C_6H_4−NC molecule on the Pt(111) surface is evaluated by a balance of σ donation (from the C lone pair orbital to the partially filled d orbitals of the metal surface) and π back-donation (from the Pt d orbitals to the NC π* orbitals). Both σ donation and π back-donation can contribute to the bond formation of the molecule with the metal surface. It is worth noting that the mixing states between MOs of adsorbate and the metal *d*-band which are outside the regime of the Blyholder model have been included in the Pettersson-Nilsson model.[77−81] This model includes additional MOs and describes the interaction between adsorbate and metal surfaces by σ-repulsion/π-attraction mechanism, and thus essentially extends the simple picture of the Blyholder model. More recently, the extended σ-repulsion/π-attraction has pointed out that the σ interaction has both attractive and

repulsive components *via* electron donation to the metal bands and the Pauli repulsion, respectively. This newly presented model has been used to explicitly explain the C−O and C−metal bond strengths of CO adsorbed on Pt−Os binary alloy and Pt−Ru−Os tertiary alloy,[82] and PtRuOsIr quaternary,[83] on PtRu alloys,[84] and Pt(100) and Ru(0001) surfaces,[85] as well as water and CO co-adsorbed on Pt(111) surface at various coverages.[86] To characterize the substituent effect on the NC stretching frequency and bond order concisely, we discuss the donation and back-donation strengths based on a localized perspective of chemical bonding in a quantitative manner.

Figure 5 shows NBOs of (a) five d orbitals of the Pt atom in the Pt(111) surface, (b) Pt−C σ bonding orbital, and (c) Pt−C σ* antibonding orbital for H−C_6H_4−NC molecule adsorbed on the Pt(111) surface. The Pt−C σ bonding and σ* antibonding orbitals consist of the C lone pair orbital of H−C_6H_4−NC in Fig. 1 and Pt d_{z^2} orbital. When the C lone pair orbital interacts with the partially filled Pt d_{z^2} orbital, electron transfer occurs from X−C_6H_4−NC molecule to the adsorbed Pt atom where Pt−C σ bonding and σ* antibonding orbitals locate around the Fermi level, as illustrated by the COHP density of states (see **Fig. S3** in SI**)**. The Pt−C σ bonding orbital is almost doubly-occupied with an occupation of above 1.95 electrons, which is consistent with the picture of a localized two-center bond. The ionic character of Pt−C bond has also been indicated by the ELF analysis (see **Fig. S4** in SI). The NBO population analysis also supports the view of this strongly ionic Pt−C bond (see **Fig. S2** in SI**)**. The natural charge of the C atom of the NC bond of H−C_6H_4−NC molecule case changes from +0.23 (isolated molecule) to +0.45 (on the surface), due to the conversion of the C atom lone pair orbital to the Pt−C bonding orbital, while the natural charge of N atom of the NC bond changes slightly from −0.46 (isolated molecule) to −0.36 (on the surface). The charge of the adsorbing Pt atom is −0.45, while the charge of the three neighboring Pt atoms on the top layer is +0.16. The charge difference (Fig. S2) between C atom and its

adsorbing Pt atom shows an increasing trend as a function of the Hammett constant, which would leads to a decrease trend in the Pt−C bond length (Fig. S5).

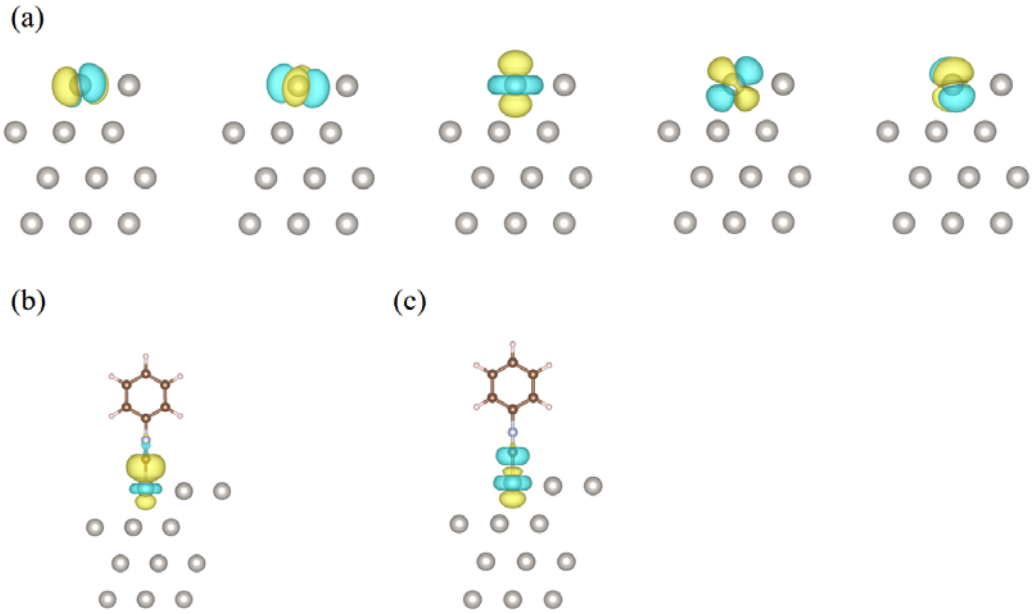

Figure 5. NBOs of (a) five d orbitals of the Pt atom in the Pt(111) surface, (b) Pt−C σ bonding orbital, and (c) Pt−C σ* antibonding orbital, which consists of the C lone pair orbital of H−C_6H_4−NC and Pt d_{z^2} orbital.

As shown in Fig. 4a, the NC stretching frequencies of the X−C_6H_4−NC molecule show a blue shift by ~70 cm^{-1} after adsorption, compared with those for the corresponding isolated molecule. This feature can be attributed to the σ donation from the C lone pair orbital of the molecule to the surface because the C lone pair orbital possesses a partial NC antibonding character, as shown in Fig. 1. The Pt−C σ bond formation by the σ donation induces the suppression of this antibonding character, leading to the strengthening of the NC bond and a blue-shift of the frequency.[87] From Fig. 4a, we also noted that the amount of blue shift in the NC stretching

frequency decreases gradually as the Hammett constant increases. **Figure 6** shows the NBO occupancies in Pt−C σ bonding orbital and σ* antibonding orbital, respectively, as a function of the Hammett constant. With the change of the Hammett constant, the NBO occupancies in Pt−C σ bonding orbital remains unchanged. In contrast, the NBO occupancies in Pt−C σ* antibonding orbital exhibits an evident linearly increasing trend. Thus, the substituent effect on the formation of Pt−C σ bond appears mainly in the change of the Pt−C σ* antibonding orbital occupancy. The increasing trend in the Pt−C σ* antibonding orbital occupancy reflects the increase of the NC antibonding character due to the C lone pair orbital. This feature is consistent with the decreasing tendency of the amount of blue-shift of the NC stretching frequency as the Hammett constant increases.

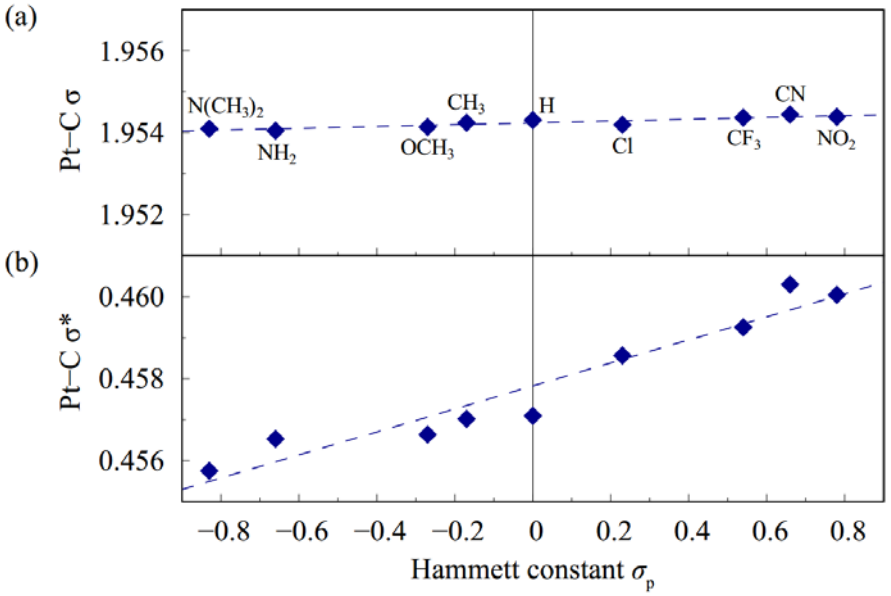

Figure 6. The NBO occupancies in (a) Pt−C σ bonding orbital and (b) Pt−C σ* antibonding orbital of X−C_6H_4−NC molecule adsorbed on the Pt surface, as a function of the Hammett constant of the substituent.

Besides the interaction between the C lone pair orbital of the NC group and Pt d orbitals, the NC σ and two π bonding orbitals also interact with the Pt d orbitals. **Figure S6** in SI shows the decreasing amount of NBO occupancy of the respective bonding orbitals after adsorbing on the surface. Each of them has fewer occupancy after adsorption (the decreasing amount of occupancy is only around 0.02~0.03). In particular, the decreasing amount of NBO occupancy of π_{vert} exhibits a decreasing trend as a function of the Hammett constant. This is ascribed to the electron donating and withdrawing ability of the substituent. In comparison with the Pt−C σ bond, the NBO occupancies in the NC σ and π orbitals do not change significantly with respect to the electron donating and withdrawing ability of the substituent. Thus, we conclude that the Pt−C bond is formed mainly from the C lone pair orbital of the isolated X−C_6H_4−NC molecule.

In the π back-donation from the Pt surface to the molecule, the NC π* orbital interacts with the Pt d-states. The partially filling of the π* orbitals upon adsorption is a typical phenomenon towards the σ donation/π back-donation model. The π back-donation reduces the NC bond strength, and therefore, gives rise to a red shift to the NC stretching frequency, which is opposite to the σ donation. Here, we define the NBO occupancy *increment* as the difference of orbital occupancy in NC π* orbitals between X−C_6H_4−NC molecules on the Pt surface and isolated X−C_6H_4−NC molecules. **Figure 7** shows the NBO occupancy *increment* for the NC π* antibonding orbitals between isolated and adsorbed X−C_6H_4−NC molecule for (a) vertical component (π^*_{vert}), and (b) parallel component (π^*_{para}); 0.20~0.30 occupancy *increment* is observed in each π* orbital equally. This nontrivial antibonding occupancy *increment* demonstrates the electron transfer from the adsorbed Pt surface to the molecule. Substituent with stronger electron withdrawing ability facilitates the filling of the π* NC orbital. In contrast, substituent with stronger electron donating ability impedes the filling of the NC π* orbital. More electron in the NC π* orbital lowers the NC

bond order. Therefore, the NC bond order behaves as an overall decreasing property, as shown in the Fig. 4b. On the other hand, we conclude that the π back-donation strength becomes larger with the increase of electron withdrawing ability of the substituent.

The occupancy change also appears in the σ* antibonding orbital (see **Fig. S7** in SI**)**. In comparison with two main π* orbitals, the occupancy *increment* in the σ* orbital is very limited (~0.009). However, it also shows the linearly increasing tendency, which can be attributed to the increase of the electron withdrawing ability of the substituent.

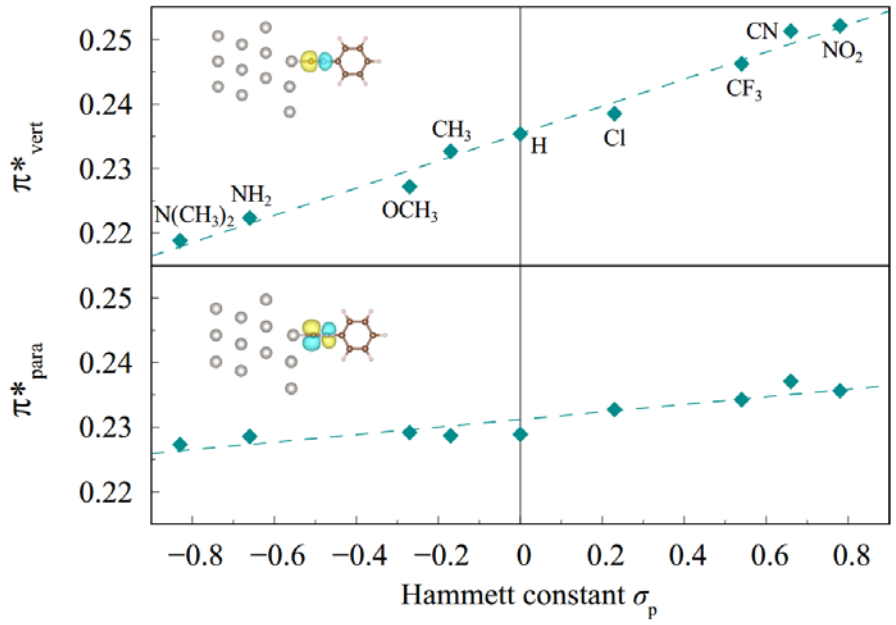

Figure 7. The NBO occupancy *increment* of the NC π* antibonding orbitals between isolated and adsorbed X−C_6H_4−NC molecule for (a) vertical component (π^*_{vert}), and (b) parallel component (π^*_{para}). The insets are the schematic configurations of these two NC π* antibonding orbitals.

The donor/acceptor analysis given by Dinnington and Schmidt[38] ascertains the source of this antibonding orbital occupancy is from the lone pairs on the adsorbing Pt. The conformation of

d orbitals of the adsorbing Pt atom has slightly inclined relative to the coordinate plane mainly due to the presence of the π-conjugated benzene. Due to symmetry restriction, the main contribution comes from the deformed d_{xz} and d_{yz} orbitals on the adsorbing Pt atom, as shown in **Fig. 8**. These two d orbitals have lobes pointing up from the Pt surface with similar symmetry as π orbitals. This shows a visual representation of the concept of metal back bonding.[88]

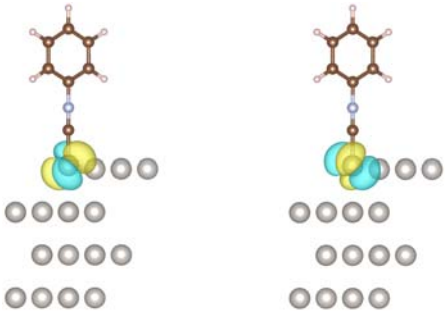

Figure 8. The deformed d_{xz} and d_{yz} orbitals on the adsorbing Pt atom.

Both σ donation and π back-donation are responsible for the change of the NC stretching frequency. The blue shift in the NC stretching frequency of the molecule on the surface is mainly due to the σ donation, whereas the red shift is caused by the π* back-donation. The overall decreasing trend of the frequency as a function of the Hammett constant is determined by a resultant effect of the donation and back-donation between molecule and surface, and electron donating and withdrawing ability of the substituent. On the other hand, a definition of NBO bond order given here determines the relatively more significant change in the NC antibonding orbitals, which caused by the π back-donation plays a dominant role while the change for orbital occupancy in the NC bonding orbitals is limited. Therefore, it can be easily understood that the bond order in the case of X−C_6H_4−NC on Pt(111) is primarily attributed to the π back-donation. The substantial decrease of the bond order change can thereby be explained in this way.

SUMMARY

In this paper, we systematically investigated the NC bond strength of the X−C_6H_4−NC molecule on the Pt surface by periodic-boundary DFT calculations, focusing on the substituent effect and the surface effect. The NC stretching frequency and NC bond order were calculated and plotted as a function of the Hammett constant of the substituents, X = $N(CH_3)_2$, NH_2, OCH_3, CH_3, H, Cl, CF_3, CN, and NO_2. The NC bond order was evaluated as the difference of NBO occupancies in the bonding and antibonding orbitals, divided by two, which were determined from the periodic implemented NBO computations. For isolated molecule, the plots of the calculated NC stretching frequency and bond order show a "volcano-like" profile, which is intuitively understandable; for the molecules on the Pt surface, the NC bonding strength is affected by the substituent through a benzene ring, as well as the σ donation and π back-donation between the molecule and surface, making it complicated to interpret the tendency in variations of the NC bond strength. The detailed analysis of NBOs clarifies the significant role of the C lone pair orbital in the NC bond of the molecule, which has a slight NC antibonding character. After adsorption, the similar decreasing trends have been obtained both for NC stretching frequency and bond order, reflecting the validity of the NBO bond order model for predict the stretching frequency variation and other conceptions concerning the bond strength. The present study demonstrated that the NBO analysis of chemical bonds of various organic molecules adsorbed on the surface can bring a deep understanding of the interaction of the molecule with the surface from the viewpoint of electronic wavefunction, which opens a new research area in the surface science field.

ACKNOWLEDGMENT

B.W. gratefully acknowledges the Ph.D. scholarship from China Scholarship Council (Grant No. 201808050073). This work was partly supported by Elements Strategy Initiative of MEXT, grant number JPMXP0112101003, the Photo-excitonix Project in Hokkaido University, JST CREST grant number JPMJCR1902, Japan and the MEXT project “Integrated Research on Chemical Synthesis”. Some of calculations were performed using the Research Center for Computational Science, Okazaki, Japan and the Academic Center for Computing and Media Studies (ACCMS) of Kyoto University.

REFERENCES

1. M. Ratner, *Nat. Nanotechnol*., 2013, **8**, 378−381.
2. L. Sun, Y. A. Diaz-Fernandez, T. A. Gschneidtner, F. Westerlund, S. Lara-Avila and K. Moth-Poulsen, *Chem. Soc. Rev.*, 2014, **43**, 7378−7411.
3. D. Xiang, X. Wang, C. Jia, T. Lee and X. Guo, *Chem. Rev.*, 2016, **116**, 4318−4440.
4. C. Jia and X. Guo, *Chem. Soc. Rev.*, 2013, **42**, 5642−5660.
5. S. Casalini, C. A. Bortolotti, F. Leonardi and F. Biscarini, *Chem. Soc. Rev.*, 2016, **46**, 40−71.
6. K. Wang, B. Xu, *Top. Curr. Chem*., 2017, **375**, 17.
7. D. Olson, A. Boscoboinik and W.T. Tysoe, *Chem. Commun.*, 2019, **55**, 13872−13875.
8. S. Watson, M. Nie, L. Wang and K. Stokes, *RSC Adv.*, 2015, **5**, 89698−89730.
9. E. Leary, A. La Rosa, M. T. González, G. Rubio-Bollinger, N. Agraït and N. Martín, *Chem. Soc. Rev.*, 2015, **44**, 920−942.
10. T. A. Su, M. Neupane, M. L. Steigerwald, L. Venkataraman and C. Nuckolls, *Nat. Rev. Mater.*, 2016, **1**, 16002.
11. S. Ahn, S. V. Aradhya, R. S. Klausen, B. Capozzi, X. Roy, M. L. Steigerwald, C. Nuckolls and L. Venkataraman, *Phys. Chem. Chem. Phys*., 2012, **14**, 13841−13845.
12. J. C. Love, L. A. Estroff, J. K. Kriebel, R. G. Nuzzo and G. M. Whitesides, *Chem. Rev.*, 2005, **105**, 1103−1170.
13. K. Uosaki, T. Kondo, X. Q. Zhang and M. Yanagida, *J. Am. Chem. Soc.*, 1997, **119**, 8367.
14. C. Vericat, M. E. Vela, G. Benitez, P. Carro and R. C. Salvarezza, *Chem. Soc. Rev.*, 2010, **39**, 1805−1834.
15. A. de Melo Souza, I. Rungger, R. B. Pontes, A. R. Rocha, A. J. R. da Silva, U. Schwingenschlöegl and S. Sanvito, *Nanoscale*, 2014, **6**, 14495.

16. K. Horiguchi, M. Tsutsui, S. Kurokawa and A. Sakai, *Nanotechnology*, 2009, **20**, 025204.

17. K. Ikeda, S. Suzuki and K. Uosaki, *Nano Lett.*, 2011, **11**, 1716−1722.

18. M. Inagaki, K. Motobayashi and K. Ikeda, *J. Phys. Chem. Lett.*, 2017, **8**, 4236−4240.

19. K. Ikeda, Y. Takeuchi, K. Kanamaru, S. Suzuki and K. Uosaki, *J. Phys. Chem. C*, 2016, **120**, 15823−15829.

20. B. Kim, J. M. Beebe, Y. Jun, X.-Y. Zhu and C. D. Frisbie, *J. Am. Chem. Soc.*, 2006, **128**, 4970−4971.

21. M. Kiguchi, S. Miura, K. Hara, M. Sawamura and K. Murakoshi, *App l. Phys. Lett.*, 2006, **89**, 213104.

22. M. Ito, H. Noguchi, K. Ikeda and K. Uosaki, *Phys. Chem. Chem. Phys.*, 2010, **12**, 3156−3163.

23. J. Hu, M. Tanabe, J. Sato, K. Uosaki and K. Ikeda, *J. Am. Chem. Soc.*, 2014, **136**, 10299−10307.

24. J. Hu, N. Hoshi, K. Uosaki and K. Ikeda, *Nano Lett.*, 2015, **15**, 7982−7986.

25. K. Ikeda, N. Fujimoto and K. Uosaki, *J. Phys. Chem. C*, 2014, **118**, 21550.

26. K. Ikeda, J. Sato and K. Uosaki, *J. Photochem. Photobiol., A*, 2011, **221**, 175−180.

27. K. Ikeda, A. Kimura and K. Uosaki, *J. Electroanal. Chem.*, 2017, **800**, 151−155.

28. K. Ikeda, J. Sato, N. Fujimoto, N. Hayazawa, S. Kawata and K. Uosaki, *J. Phys. Chem. C*, 2009, **113**, 11816−11821.

29. K. Ikeda, N. Fujimoto, H. Uehara and K. Uosaki, *Chem. Phys. Lett.*, 2008, **460**, 205−208.

30. W. Hu, S. Duan, Y. Zhang, H. Ren, J. Jiang and Y. Luo, *Phys. Chem. Chem. Phys.*, 2017, **19**, 32389−32397. (NC)

31. R. F. W. Bader, *Chem. Rev.*, 1991, **91**, 893−928.

32. R. F. W. Bader, *Atoms in Molecules: A Quantum Theory*, Oxford University Press, USA, 1994.

33. R. F. W. Bader, *Acc. Chem. Res.*, 1985, **18**, 9−15.

34. R. F. W. Bader. In: P. v. Schleyer, (Ed.). Encyclopedia of Computational Chemistry. (John Wiley and Sons, Chichester, U.K., 1998), pp. 64−86.

35. A. D. Becke and K. E. Edgecombe, *J. Chem. Phys.*, 1990, **92**, 5397−5403.

36. A. Savin, R. Nesper, S. Wengert and T. F. Fässler, A*ngew. Chem., Int. Ed. Engl.,* 1997, **36**, 1808.

37. F. Weinhold and C. Landis, *Valency and Bonding–A Natural Bond Orbital Donor-Acceptor Perspective*; Cambridge University Press: Cambridge, 2005; pp 1−44.

38. B. D. Dunnington and J. R. Schmidt, *J. Chem. Theory Comput.*, 2012, **8**, 1902−1911.

39. G. T. K. K. Gunasooriya and M. Saeys, *ACS Catal.*, 2018, **8**, 3770−3774.

40. I. A. Popov, E. Jimenez-Izal, A. N. Alexandrova and A. I. Boldyrev, *J. Phys. Chem. C*, 2018, **122**, 11933−11937.

41. J. Jin, N. Sun, W. Hu, H. Yuan, H. F. Wang and P. Hu, *ACS Catal.*, 2018, **8**, 5415−5424.

42. P. E. Blöchl, *Phys. Rev. B*, 1994, **50**, 17953−17979.

43. G. Kresse and D. Joubert, *Phys. Rev. B*, 1999, **59**, 1758−1775.

44. G. Kresse and J. Hafner, *Phys. Rev. B*, 1993, **47**, 558−561.

45. G. Kresse and J. Hafner, *Phys. Rev. B*, 1994, **49**, 14251−14269.

46. G. Kresse and J. Furthmüller, *Phys. Rev. B*, 1996, **54**, 11169−11186.

47. G. Kresse and J. Furthmüller, *Comput. Mater. Sci.*, 1996, **6**, 15−50.

48. J. P. Perdew, K. Burke and M. Ernzerhof, *Phys. Rev. Lett.*, 1996, **77**, 3865.

49. J. P. Perdew, K. Burke and M. Ernzerhof, *Phys. Rev. Lett.*, 1997, **78**, 1396−1396.

50. S. Grimme, J. Antony, S. Ehrlich and H. Krieg, *J. Chem. Phys*., 2010, **132**, 154104.

51. A. K. Grimme, Homepage. http://www.thch.uni-bonn.de/tc/.

52. A. Antony, C. Hakanoglu, A. Asthagiri and J. F. Weaver, *J. Chem. Phys*., 2012, **136**, 054702.

53. H. J. Monkhorst and J. D. Pack, *Phys. Rev. B*, 1976, **13**, 5188−5192.

54. F. Birch, *Phys. Rev.*, 1947, **71**, 809.

55. Y. Waseda, K. Hirata and M. Ohtani, *High Temp. High Pressures*, 1975, **7**, 221.

56. D. Feller, *J. Comput. Chem.*, 1996, **17**, 1571−1586.

57. K. L. Schuchardt, B. T. Didier, T. Elsethagen, L. Sun, V. Gurumoorthi, J. Chase, J. Li and T. L. Windus, *J. Chem. Inf. Model.*, 2007, **47**, 1045−1052.

58. R. Krishnan, J. S. Binkley, R. Seeger and J. A. Pople, *J. Chem. Phys.*, 1980, **72**, 650−654.

59. A. D. McLean and G. S. Chandler, *J. Chem. Phys.*, 1980, **72**, 5639−5648.

60. R. C. de Berrêdo and F. E. Jorge, *J. Mol. Struct.: THEOCHEM*, 2010, **961**, 107−112.

61. K. Momma and F. Izumi, *J. Appl. Crystallogr.*, 2011, **44**, 1272−1276.

62. R. Dronskowski and P. E. Blöchl, *J. Phys. Chem.*, 1993, **97**, 8617−8624.

63. V. L. Deringer, A. L. Tchougréeff and R. Dronskowski, *J. Phys. Chem. A*, 2011, **115**, 5461−5466.

64. S. Maintz, V. L. Deringer, A. L. Tchougréeff and R. Dronskowski, *J. Comput. Chem.*, 2013, **34**, 2557−2567.

65. L. P. Hammett, *J. Am. Chem. Soc*., 1937, **59**, 96−103.

66. C. Hansch, A. Leo and R. W. Taft, *Chem. Rev*., 1991, **91**, 165−195.

67. P. J. Feibelman, B. Hammer, J. K. Nørskov, F. Wagner, M. Scheffler, R. Stumpf, R. Watwe and J. Dumesic, *J. Phys. Chem. B*, 2001, **105**, 4018−4025.

68. G. Kresse, A. Gil and P. Sautet, *Phys. Rev. B*, 2003, **68**, 073401.

69. Q. M. Hu, K. Reuter and M. Scheffler, *Phys. Rev. Lett.*, 2007, **98**, 176103.

70. L. Schimka, J. Harl, A. Stroppa, A. Grüneis, M. Marsman, F. Mittendorfer and G. Kresse, *Nat. Mater.*, 2010, **9**, 741−744.

71. S. Gautier, S. N. Steinmann, C. Michel, P. Fleurat-Lessard and P. Sautet, *Phys. Chem. Chem. Phys.*, 2015, **17**, 28921−28930.

72. Y. Li, D. Lu, S. A. Swanson, J. C. Scott and G. Galli, *J. Phys. Chem. C*, 2008, **112**, 6413. (calculation valiadatity)

73. H. Aizawa and S. Tsuneyuki, *Surface Science*, 1998, **399**, 364−370.

74. G. Blyholder, *J. Phys. Chem.*, 1964, **68**, 2772−2777.

75. S. S. Sung and R. Hoffmann, *J. Am. Chem. Soc.*, 1985, **107**, 578−584.

76. Y. Gilman, P. B. Allen and M. S. Hybertsen, *J. Phys. Chem. C*, 2008, **112**, 3314−3320.

77. P. Bennich, T. Wiell, O. Karis, M. Weinelt, N. Wassdahl, A. Nilsson, M. Nyberg, L. G. M. Pettersson, J. Stohr and M. Samant, *Phys. Rev. B*, 1998, **57**, 9274.

78. A. Föhlisch, M. Nyberg, J. Hasselström, O. Karis, L. G. M. Pettersson and A. Nilsson, *Phys. Rev. Lett.*, 2000, **85**, 3309−3312.

79. A. Föhlisch, M. Nyberg, P. Bennich, L. Triguero, J. Hasselström, O. Karis, L. G. M. Pettersson, and A. Nilsson, *J. Chem. Phys*., 2000, **112**, 1946.

80. A. Nilsson, M. Weinelt, T. Wiell, P. Bennich, O. Karis, N. Wassdahl, J. Stohr, and M. G. Samant, *Phys. Rev. Lett*., 1997, **78**, 2847.

81. K. M. Gameel, I. M. Sharafeldin and N. K. Allam, *Phys. Chem. Chem. Phys.*, 2019, **21**, 11476–11487.

82. N. Dimakis, T. Mion, and E. S. Smotkin, *J. Phys. Chem. C*, 2012, **116**, 21447.

83. N. Dimakis, F. A. Flor, N. E. Navarro, A. Salgado, and E. S. Smotkin, *J. Phys. Chem. C*, 2016, **120**, 10427.

84. N. Dimakis, M. Cowan, G. Hanson and E. S. Smotkin, *J. Phys. Chem. C*, 2009, **113**, 18730−18739.

85. N. Dimakis, N. E. Navarro, T. Mion and E. S. Smotkin, *J. Phys. Chem. C*, 2014, **118**, 11711−11722.
86. N. Dimakis, I. Salas, L. Gonzalez, N. Loupe and E. S. Smotkin, *J. Chem. Phys*., 2019, **150**, 024703.
87. D. Astruc, Organometallic Chemistry and Catalysis, 608 pp. Springer, Berlin, 2007.
88. R. Hoffmann, Solids and Surfaces: A Chemist's View of Bonding in Extended Structures; VCH Publishers: New York, 1988.

Graphical Abstract